

Deglacial export of pre-aged terrigenous carbon to the Bay of Biscay

Eduardo Queiroz Alves^{1,†}, Wanyee Wong^{1,2,‡}, Jens Hefter¹, Hendrik Grotheer^{1,4}, Tommaso Tesi³, Torben Gentz¹, Karin Zonneveld⁴, and Gesine Mollenhauer^{1,2,4}

¹Alfred Wegener Institute for Polar and Marine Research, Bremerhaven, Germany

²University of Bremen, Bremen, Germany

³Institute of Polar Sciences - National Research Council, Bologna, Italy

⁴MARUM-Center for Marine Environmental Sciences, University of Bremen, Bremen, Germany

[†]now at Departamento de Geoquímica, Universidade Federal Fluminense, Brazil

[‡]now at NORCE Norwegian Research Centre, Bjerknnes Centre for Climate Research, Bergen, Norway

Correspondence: Eduardo Queiroz Alves (eduardo.queiroz.alves@awi.de)

Abstract. The last deglaciation is the most recent relatively well-documented period of pronounced and fast climate warming and, as such, it holds important information for our understanding of the climate system. Notably, while research into terrestrial organic carbon reservoirs has been instrumental in exploring the possible sources of atmospheric carbon dioxide during periods of rapid change, the underlying mechanisms are not fully understood. Here we investigate the mobilization of organic matter to the Bay of Biscay, located in the northeastern Atlantic Ocean off the coasts of France and Spain. Specifically, we focus on the area that was the mouth of the Channel River during the last deglaciation, where an enhanced terrigenous input has been reported for the last glacial-interglacial transition. We conducted a comprehensive suite of biomarker analyses (e.g., *n*-alkanes, hopanes, and *n*-alkanoic acids) and isotopic investigations (radiocarbon dating and $\delta^{13}\text{C}$ measurements) on a high-resolution sedimentary archive. The present study provides the first direct evidence for the fluvial supply of immature and ancient terrestrial organic matter to the core location. Moreover, our results reveal the possibility of permafrost carbon export to the ocean, driven by processes such as deglacial warming and glacial erosion. These findings are consistent with observations from other regions characterized by present or past permafrost conditions on land, which have shown that permafrost thaw and glacial erosion can lead to carbon remobilization, potentially influencing atmospheric carbon dioxide levels.

1 Introduction

High-latitude permafrost soils hold ca. 1000 Pg of soil organic carbon (C) in the upper 3 m of the northern circumpolar region (Hugelius et al., 2014). This immense amount of C is in the form of frozen organic matter (OM), the thawing of which releases greenhouse gases, inducing positive feedback mechanisms that have implications for the C cycle on a global scale (Zimov et al., 2006; Schuur et al., 2008, 2009; Hugelius et al., 2014; Schuur et al., 2015). While current climate change raises concerns about the stability of these massive pools of organic C (Vonk et al., 2012; Schneider Von Deimling et al., 2015), the dynamic character of Earth's climate means that past trends and variability can be examined to improve future projections of this effect. The hypothesis of a combined contribution of ancient terrestrial C, potentially derived from thawing permafrost, and marine C sources to elevated atmospheric levels of carbon dioxide (CO_2) and methane (CH_4) during the last deglaciation is discussed in

several studies (Ciais et al., 2012; Köhler et al., 2014; Bauska et al., 2016; Crichton et al., 2016; Simmons et al., 2016). Over the course of the Last Glacial Maximum (LGM), large expanses of continuous permafrost were found in the Eurasian continent, covering much of central and western Europe, in areas where permafrost cover today no longer exists (Vandenberghe and Pissart, 1993; Levavasseur et al., 2011; Vandenberghe et al., 2012; Žák et al., 2012; Schaefer et al., 2014; Vandenberghe et al., 2014) (Figure 1). These regions comprise the southern edge of the LGM permafrost area and, according to Köhler et al. (2014), are likely to have experienced a rapid loss of massive amounts of ancient C as a result of thawing during the last deglaciation. However, while direct evidence for the deglacial remobilization of ancient C from permafrost has been reported for the Arctic (Tesi et al., 2016; Keskitalo et al., 2017; Martens et al., 2019, 2020; Wu et al., 2022) and subarctic (Winterfeld et al., 2018; Meyer et al., 2019), similar data are still lacking for the European realm where the phenomenon has been suggested on the basis of enhanced terrigenous biomarker concentrations in sediment cores (Ménot et al., 2006; Rostek and Bard, 2013; Soulet et al., 2013).

During the LGM, continental glaciers were part of the European landscape. The Fennoscandian (FIS) and the British-Irish (BIIS) ice sheets covered most of Britain, Ireland, Northern Europe and the North Sea (Bowen et al., 2002; Svendsen et al., 2004; Mangerud et al., 2004), contributing to the lower eustatic sea level and altering coastlines (e.g., Fairbanks, 1989; Lambeck, 1997; Lambeck et al., 2014). This sea-level lowstand, paired with the configuration of the BIIS and the FIS, led to a reorganization of major European drainage basins, with continental runoff being funnelled through the English Channel (Gibbard, 1988). The so-called Fleuve Manche or Channel River received the runoff of major European rivers, carrying meltwaters from glaciers and ice sheets (e.g., Antoine et al., 2003; Bourillet et al., 2003) (Figure 1). As a consequence, changes in the hydrological cycle in Europe during the last glacial-interglacial transition induced a strong response from this system, resulting in increased water flow in the Channel River and its tributaries (e.g., Ménot et al., 2006; Toucanne et al., 2009, 2010). Permafrost developed in the glacier-free areas of the continent and towards the end of the last glaciation it is likely to have reached its maximum extent, with discontinuous permafrost present in regions almost as far south as the Mediterranean Sea (Vandenberghe et al., 2014).

Permafrost encompasses a diverse range of organic-rich deposits, including ancient peat, organic-rich soils, and potentially mineral soils, all of which can become stabilized (frozen) under permafrost conditions, preserving C within them. There is evidence for the presence of several peatlands with active peat deposition in northern latitudes ($> 40^{\circ}\text{N}$), including Northern Europe, during the last interglacial (130 - 116 kyr BP; Treat et al., 2019). Although the occurrence of permafrost during the LGM likely resulted in the long-term burial of peatland OM, deglacial permafrost thawing may have led to the fluvial export of peat-derived OM to the ocean (see e.g., Schefuß et al., 2016; Garcin et al., 2022). In addition to permafrost, petrogenic material carried by glacial meltwater may have been another source of fossil OM to the oceans during the last deglaciation. Following glacial retreat, the mechanical erosion of bedrock such as oil shales mobilizes petrogenic C, which is transported as finely ground glacial meal to the oceans (Koppes and Hallet, 2002, 2006). Therefore, if we are to accurately quantify the impact of the permafrost C feedback on Earth's climate, it is imperative to distinguish between the possible origins of the OM deposited on the continental margins over the course of the last deglaciation. Considering the presence of shale formations in Europe (e.g., Zhao et al., 2022), our study explores two primary hypotheses regarding the origin of OM: permafrost-derived

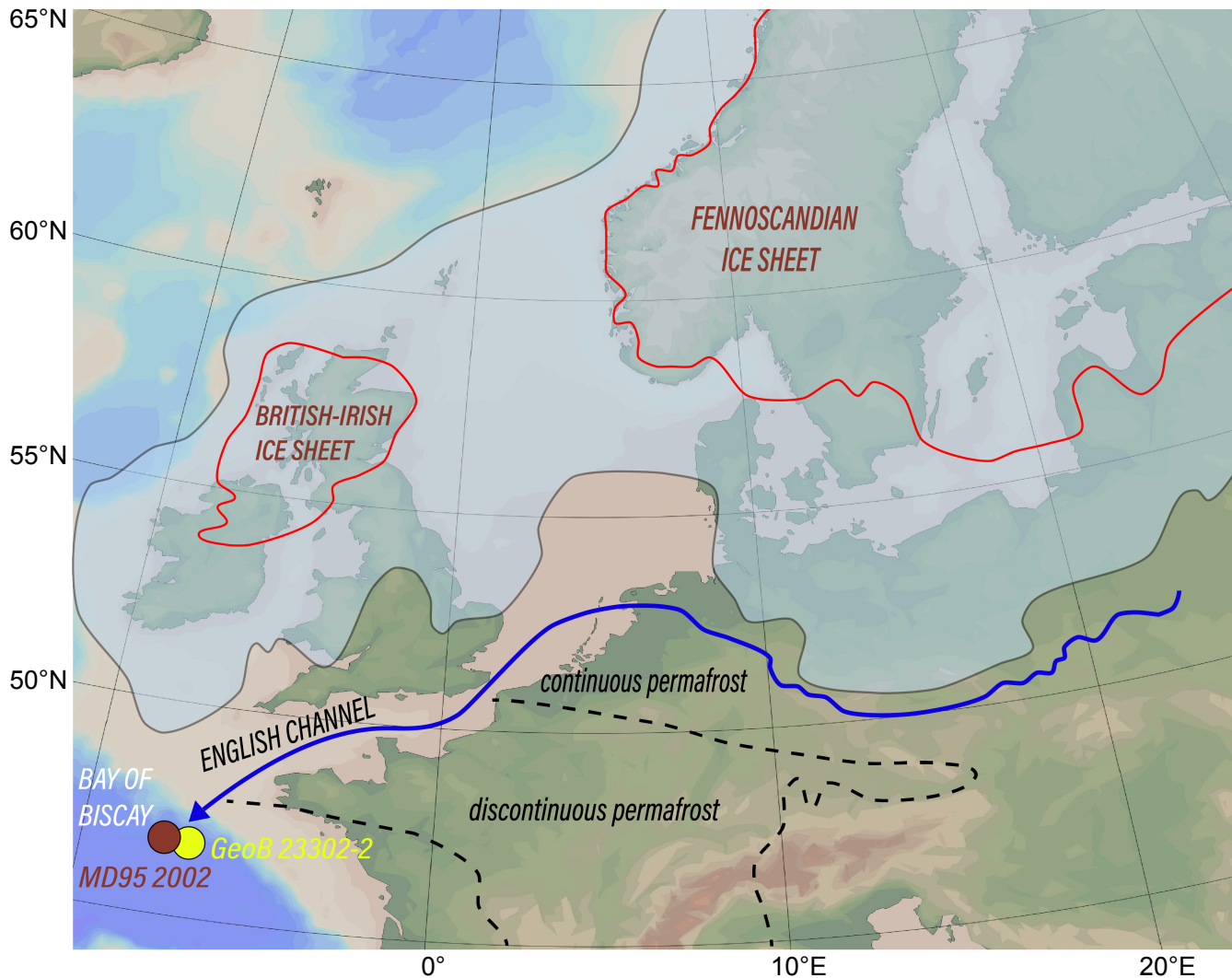


Figure 1. Northwest Europe during the LGM. The blue arrow indicates the downstream course of the Channel River from the eastern flank of the FIS. The dashed lines show the distribution of permafrost (Renssen and Vandenberghe, 2003, and references therein) and the red contours indicate the approximate limits of the ice sheets at ca. 17 ka BP (Patton et al., 2017). The yellow dot illustrates the location where core GeoB23302-2, used in the present study, was retrieved. Map based on that in Ménot et al. (2006), who studied core MD95 2002 from a nearby location (red dot).

OM, which includes peat preserved in past permafrost-covered European regions, and OM originating from petrogenic sources. Here, we analyzed organic biomarkers and conducted compound-specific radiocarbon (^{14}C) measurements on *n*-alkanoic acids isolated from a high-resolution, well-dated marine sediment core retrieved from the Channel River outflow to evaluate these hypotheses.

2 Materials and methods

Herein, we provide an overview of our analytical approach; for in-depth descriptions of each method and the specific details of our analyses, please refer to the following subsections. All the elemental, isotopic and biomarker analyses described in this section were conducted as part of the present study. In this research we used several analytical tools to examine core GeoB23302-2 (47°26.61'N, 8°28.67'W; 2167 m water depth) (Figure 1). The chronology of the sedimentary sequence was established using an age-depth model constructed with the ^{14}C ages of planktic foraminifera in the OxCal software (Bronk Ramsey, 1995, 2009a). Elemental ratios were obtained through X-ray fluorescence (XRF) core scanning. The coarse fraction of sediments tends to be enriched in zirconium (Zr), while rubidium (Rb) is found in fine-grained minerals. Therefore, here we report the ratio Zr/Rb as an elemental measure of grain size, which has been used as a proxy for river runoff (Dypvik and Harris, 2001; Kylander et al., 2011; Wang et al., 2011; Wu et al., 2020). Similarly, given that iron (Fe) is normally associated with continental weathering products and that the calcium (Ca) content in the sediment primarily reflects the presence of marine carbonate, here we use the Fe/Ca ratio as a provenance indicator, reflecting variations in terrigenous sediment delivery (Arz et al., 1999; Itambi et al., 2009; Dickson et al., 2010; Perez et al., 2016). We analysed lipid biomarkers using solvent extraction and gas chromatography and calculated *n*-alkane-derived indices, namely the carbon-number preference index (CPI_{alk}) (e.g., Bray and Evans, 1961; Marzi et al., 1993) and the proxy ratio P_{aq} (Ficken et al., 2000), which are commonly used in environmental investigations (e.g., Nichols et al., 2006; Rommerskirchen et al., 2006; Zhou et al., 2012; He et al., 2020; Feurdean et al., 2021) to assess the degree of OM degradation and reconstruct the temporal evolution of continental vegetation systems, respectively. The CPI_{alk} is based on the ratio of odd to even *n*-alkanes, providing information about the distribution of these compounds in the samples, while the P_{aq} reflects the predominance of long-chain *n*-alkanes in terrestrial vascular plants as opposed to algae and macrophytes, which primarily synthesize short- to mid-chain *n*-alkanes (Bianchi and Canuel, 2011). The P_{aq} ratio indicates the relative input of aquatic macrophytes and terrestrial plants to the sediment (Ficken et al., 2000). The prevalence of odd-numbered *n*-alkanes in fresh material implies that the CPI_{alk} can serve as an indicator of OM degradation (Bray and Evans, 1961; Marzi et al., 1993; Meyers and Ishiwatari, 1993). To further assess the presence of petrogenic OM, we used the fractional abundance of hopanes of biological origin, e.g., bacteria-derived hopanes, in relation to their diagenetic isomers ($f\beta\beta$) (Meyer et al., 2019). Here, the branched and isoprenoid tetraether (BIT) index (Hopmans et al., 2004), based on the relative abundance of branched glycerol dialkyl glycerol tetraether lipids (GDGTs) characteristic of terrestrial bacteria and crenarchaeol produced by marine Thaumarchaeota, is used as a proxy for the input of terrestrially-sourced OM. Carbon isotope analysis ($\delta^{13}\text{C}$) of bulk samples was conducted as part of our investigation into their origin. Finally, given that the results of bulk ^{14}C dating reflect the ^{14}C content of a heterogeneous mixture of compounds possibly derived from distinct sources, here we further address the provenance of the OM by using compound-specific ^{14}C analyses of high molecular weight *n*-alkanoic acids ($\text{C}_{26:0}$, $\text{C}_{28:0}$ and $\text{C}_{30:0}$) - which are typically derived from vascular plants (Bianchi and Canuel, 2011) - from specific depths in the core. This approach has been successfully employed for the identification of ancient terrigenous material export at other sites (e.g., Winterfeld et al., 2018; Meyer et al., 2019; Wu et al., 2022).

95 2.1 Sampling and core chronology

Core GeoB23302-2 was recovered from the Celtic Margin, off the English Channel (47°26.61'N, 8°28.67'W; 2167 m water depth) (Figure 1), with the help of a gravity corer during cruise MSM 79 of the research vessel Maria S. Merian. The core location is in close proximity to the site where core MD95 2002, which has been studied in previous publications (e.g., Ménot et al., 2006; Toucanne et al., 2015), was retrieved (47°27'N, 8°32'W) (see Figure 1). The chronology of our 700 cm core was established based on seven radiocarbon accelerator mass spectrometry (¹⁴C-AMS) measurements of planktic foraminifera (*G. bulloides* and *N. pachyderma*) picked at specific depths (Table 1). The preparation and measurement of these samples followed well-established protocols routinely run at the MICADAS ¹⁴C laboratory of the Alfred Wegener Institute (AWI) (Mollenhauer et al., 2021). The ¹⁴C ages were uploaded to the OxCal software version 4.4.2 (Bronk Ramsey, 1995, 2009a), and assuming that the deposition is a Poisson process, the P Sequence model was employed for the construction of an age-depth model for core GeoB23302-2 (Bronk Ramsey, 2008; Bronk Ramsey and Lee, 2013). This deposition model (Figure 2 in the Supplementary Material) uses the global marine calibration curve Marine20 (Heaton et al., 2020), and a local marine reservoir correction ΔR of 94 ± 45 ¹⁴C yr (Tisnérat-Laborde et al., 2010). It is important to note that while Marine20 incorporates larger MRA estimates for the last glacial period than Marine13, these estimates are considered more realistic due to methodological improvements in the former (Heaton et al., 2020, 2023). A general outlier analysis was employed to account for possible outliers within the chronological model (Bronk Ramsey, 2009b). The code is available in the supplementary material accompanying this paper.

2.2 Elemental analyses

The XRF characterization of core GeoB23302-2 was performed using the XRF Core Scanner II (AVAATECH Serial No. 2) at the Center for Marine Environmental Sciences (MARUM), University of Bremen, Germany. Measurements were performed at 1 cm intervals for the upper 3.5 m of the core and at every 2 cm for the remaining section. The scan resolution was set to 1 cm with 2 running rounds, during which the elements were detected with 10 and 30 kV of tube voltage. In order to account for the closed sum effects of water content, grain size and OM amount (e.g., Weltje and Tjallingii, 2008), we report the elemental ratios Zr/Rb and Fe/Ca.

2.3 Biomarker analyses and derived indices

Sediment samples taken at 10 cm intervals from core GeoB23302-2 were freeze-dried and homogenized. For each depth, approximately 3 g of sediment were subsampled and underwent ultrasonic extraction with a mixture of dichloromethane:methanol 9:1 (v:v). This step was repeated three times and the total lipid extracts obtained were then saponified with 0.1 M potassium hydroxide (KOH) in methanol:water 9:1 at 80 °C for 2 h. This procedure resulted in the separation of the neutral lipids and *n*-alkanoic acids fractions, which were subsequently extracted using *n*-hexane and dichloromethane (at pH 1), respectively. Next, silica gel chromatography was employed to further split the neutral lipids via elution with *n*-hexane and dichloromethane:methanol 1:1 (v:v), yielding the *n*-alkanes and GDGTs subfractions, respectively. The *n*-alkane concentrations were measured via gas chromatography (GC) using a 7890A GC (Agilent Technologies) equipped with a flame ionization

detector (FID) and DB-5MS fused silica capillary columns (60 m, ID 250 μm , 0.25 μm film coupled to a 5 m, ID 530 μm deactivated fused silica precolumn). Retention times and the comparison with an *n*-alkane standard were used for the identification of different compounds whereas quantifications were achieved through the use of an internal standard (squalane) added to the sample prior to extraction. We calculated *n*-alkane-derived indices, namely the CPI_{alk} (e.g., Bray and Evans, 1961; Marzi et al., 1993):

$$\text{CPI}_{alk} = \frac{1}{2} \cdot \left(\frac{C_{25} + C_{27} + C_{29} + C_{31} + C_{33}}{C_{24} + C_{26} + C_{28} + C_{30} + C_{32}} + \frac{C_{25} + C_{27} + C_{29} + C_{31} + C_{33}}{C_{26} + C_{28} + C_{30} + C_{32} + C_{34}} \right), \quad (1)$$

135

and the P_{aq} (Ficken et al., 2000):

$$P_{aq} = \frac{C_{23} + C_{25}}{C_{23} + C_{25} + C_{29} + C_{31}}, \quad (2)$$

140 Hopanes were analyzed via GC coupled with time of flight mass spectrometry (GC-TOF-MS) and such a system consisted of a LECO Pegasus III (LECO Corp., St. Joseph, MI) interfaced to an Agilent 6890 GC which was equipped with a temperature programmable cooled injection system (CIS4, Gerstel). The measurements were performed using the instrumental setup described in Hefter (2008) and identification was achieved through the relative retention times and mass spectra. The sum of m/z 191 and 205 was used for the quantification of homohopane isomers (C_{31}), namely the $17\beta,21\beta$ (H), 22R homohopane, 145 the $17\beta,21\alpha$ (H), 22R + $17\beta,21\alpha$ (H), 22S homohopanes, the $17\alpha,21\beta$ (H), 22R homohopane, and the $17\alpha,21\beta$ (H), 22S homohopane. Next, the $f\beta\beta$ was calculated (Meyer et al., 2019):

$$f\beta\beta = \frac{C_{31}\beta\beta R}{C_{31}\beta\beta R + C_{31}\alpha\beta S + C_{31}\alpha\beta R + C_{31}\beta\alpha S + C_{31}\beta\alpha R} \quad (3)$$

150

The analyses of branched and isoprenoid GDGTs by High Performance Liquid Chromatography (HPLC) were performed on an Agilent 1200 series HPLC system coupled to an Agilent 6120 single quadrupole MS via an atmospheric pressure chemical ionization interface (APCI), broadly following the method described in Hopmans et al. (2016). The chromatographic separation of individual GDGTs was achieved via the use of two UPLC silica columns in series (Waters Acquity BEH HILIC, 2.1 mm x 150 mm, 1.7 μm and a 2.1 mm x 5 mm pre-column of the same material) maintained at 30 °C. Positive-ion APCI-MS 155

and selective ion monitoring (SIM) of (M+H)⁺ ions (Sinninghe Damsté et al., 2000) or ion-source fragmentation products of OH-GDGTs (Liu et al., 2012) allowed the identification of GDGTs. Quantification was performed with the use of an internal standard (C₄₆-GDGT) added prior to extraction. For this research, we calculated the BIT index (Hopmans et al., 2004):

$$160 \quad BIT = \frac{I + II + III}{I + II + III + cren} \quad (4)$$

where the roman numerals refer to specific GDGTs characteristic of terrestrial bacteria and cren stands for crenarchaeol, which is derived from marine planktonic Thaumarchaeota.

165 **2.4 Compound-specific radiocarbon analyses (CSRA)**

Soxhlet extraction was employed for the compound-specific ¹⁴C dating of high molecular weight *n*-alkanoic acids. For that purpose, approximately 100 g of freeze-dried and homogenized sediment taken from selected depths in core GeoB23302-2 were extracted for 48 h using a mixture of dichloromethane:methanol 9:1 (v:v). Total lipid extracts were saponified with 0.1 M KOH in methanol:water 9:1 at 80 °C for 2 h and the *n*-alkanoic acids were recovered from the saponified solution using *n*-hexane at pH 1. Next, *n*-alkanoic acids were methylated at 80 °C overnight in a nitrogen atmosphere with HCl and methanol of known ¹⁴C signature to yield the fatty acid methyl esters (FAMES) that were later extracted with *n*-hexane. Silica gel chromatography was employed to separate FAMES from polar compounds. The *n*-C_{26:0}, *n*-C_{28:0} and *n*-C_{30:0} alkanolic acids underwent purification via preparative capillary GC (PC-GC; Eglinton et al., 1996) on an Agilent HP6890N GC with a Gerstel Cooled Injection System (CIS) connected to a Gerstel preparative fraction collector (Kusch et al., 2010). A Restek
175 Rxi-1ms fused silica capillary column (30 m, 0.53 mm diameter, 1.5 μm film thickness) equipped the GC. Injection was performed stepwise with 5 μL per injection and, at the end of the process, the purity of the FAMES was checked by analyzing aliquots of the samples via GC-FID. The purified FAMES were transferred to tin capsules (25 μL volume; ELEMENTAR) using dichloromethane, dried on a hot plate at 40 °C and packed. An Elementar vario ISOTOPE EA (Elemental Analyzer) was used for the combustion of the samples, generating CO₂ with carbon isotopic ratios directly determined by the connected
180 MICADAS system. Reference standards (oxalic acid II; SRM 4990C) and ¹⁴C-free CO₂ gas had their ¹⁴C content measured together with the samples. The BATS software (Wacker et al., 2010) was used for blank corrections and standard normalization and the final results are reported as fraction modern carbon (F_m).

2.5 Assessment and correction of CSRA procedure blank

The preparation procedures for CSRA introduce exogenous C, i.e., contaminants, to samples. The degree of contamination varies according to the methods employed and, in our case, processes such as column bleed and carry-over during prep-GC
185 compound isolation may contribute to this. For this reason, assessing the F_m and the size of the blank (F_{mblank} and m_{blank},

respectively) is essential for accurate results. Here, in-house reference samples of ^{14}C -free Messel Shale ($F_m = 0$) and modern apple peel ($F_m = 1.029 \pm 0.001$) underwent the same pre-treatment as samples of unknown age and their results were used for blank correction following the method outlined in Sun et al. (2020). Isotopic mass balance was employed in order to make a
190 correction for the methyl group added during the derivatization of the samples. Uncertainties were fully propagated.

2.6 Pre-depositional ^{14}C ages of terrigenous compounds

The $\Delta^{14}\text{C}$ values of the *n*-alkanoic acids analysed here were corrected for radioactive decay between 1950 and 2021, which is the year of measurement. These values were then used to calculate the $\Delta^{14}\text{C}$ values at the time of deposition:

$$\Delta^{14}C_{initial} = \left[\left(\frac{\Delta^{14}C}{1000} + 1 \right) \cdot e^{\lambda t} - 1 \right] \cdot 1,000 \quad (5)$$

195 where λ is a decay constant ($1/8,267 \text{ yr}^{-1}$) and t is the time of deposition. The $\Delta^{14}\text{C}$ values of the atmosphere contemporaneous with the compounds ($\Delta^{14}C_{atm}$) were obtained from comparison with the IntCal20 dataset (Reimer et al., 2020) using the age ranges given by the deposition model for the respective sediment layers. Finally, pre-depositional ^{14}C ages for the *n*-alkanoic acids were given by:

$$A = -8,033 \cdot \ln \left(\frac{1 + \Delta^{14}C_{initial}/1,000}{1 + \Delta^{14}C_{atm}/1,000} \right) \quad (6)$$

200 These calculations follow the method outlined in Schefuß et al. (2016) and later in Winterfeld et al. (2018), where more details can be found.

2.7 Stable isotope analyses

Carbon stable isotope ($\delta^{13}\text{C}$) analyses were carried out on acidified samples (Ag capsules, HCl, 1.5 M) in order to remove the inorganic C (Nieuwenhuize et al., 1994). Analyses were performed using a Thermo Scientific DELTA Q Isotope Ratio
205 Mass Spectrometer coupled to a Thermo Scientific FLASH 2000 CHNS/O Analyzer via ConFlo III at the Stable Isotope Laboratory of ISP-CNR. $\delta^{13}\text{C}$ data are expressed in the conventional delta notation (‰). Isotopic data were calibrated using the IAEA reference material IAEA-CH7 polyethylene, -32.15‰vs VPDB). Throughout the runs, we used other standards with a sediment matrix routinely used in the laboratory to check the reproducibility of measurements. The standard deviation for $\delta^{13}\text{C}$ measurements was lower than $\pm 0.1\text{‰}$ based on replicates of sediment standards.

210 3 Results

The GeoB23302-2 sediment core spans a period from approximately 25 to 4 kcal BP (Table 1). The age-depth model for this core shows a period of enhanced deposition between approximately 20 and 15 kcal BP (Figure 2 in the Supplementary Material). An outlier analysis shows that the model represents well the foraminifera ^{14}C ages, with an OxCal overall agreement

index of 99%. From approximately 20.6 until 15 kcal BP, the Zr/Rb ratio shows a long-term increase, whereas a period of relatively high Fe/Ca values is observed at ca. 21 - 16.4 kcal BP (Figure 2c). Values for the proxy P_{aq} are relatively low during the LGM and show a pronounced increase at approximately 21 kcal BP with higher values towards the late glacial and a sudden decrease at the onset of Heinrich event 1 (iceberg discharge from the Laurentide ice sheet into the North Atlantic Ocean; H1; ca. 17.2 kcal BP) (Figure 2d). This is followed by a sharp increase at approximately 16.5 kcal BP and a drop to Holocene values around 16.3 kcal BP. The CPI_{alk} and the $f\beta\beta$ proxy show relatively low values in the late glacial/early deglaciation when compared to the Holocene (Figure 2e). During the LGM, the CPI_{alk} values are broadly constant while an increase is observed at the beginning of H1 followed by a sharp drop around 16.5 kcal BP and a return to higher values at approximately 16.2 kcal BP. The $f\beta\beta$ record shows fluctuations during the LGM, followed by a gradual decrease starting at approximately 18 kcal BP and a sharp drop around 16.5 kcal BP before returning to higher values at approximately 16.2 kcal BP (Figure 2e). The ^{14}C ages of the long chain *n*-alkanoic acids varied from approximately 10 to 39 ^{14}C kyr. When converted to pre-depositional age estimates, it is possible to observe that at the peak of our BIT record, around 18 kcal BP, compounds pre-aged by up to ca. 25,000 ^{14}C yr were delivered to the continental slope (Figure 2f). Pre-depositional ages broadly follow the BIT record, with younger compounds observed from the end of the BIT peak (ca. 16 kcal BP) towards the Holocene. The results of our bulk $\delta^{13}C$ analyses corroborate the BIT index record, showing that terrestrial C dominantly contributed to samples during the period of enhanced terrigenous deposition, while the OM in Holocene samples is mostly marine (Table 2).

Table 1. Radiocarbon and modelled ages of planktic foraminifera picked from core GeoB23302-2.

Depth (cm)	Species	^{14}C age (^{14}C yr)	Modelled age (cal BP; 2σ)
3-4	<i>G. bulloides</i>	3556 ± 67	3600 - 3100
118-119	<i>G. bulloides</i>	9981 ± 105	11300 - 10600
234-235	<i>N. pachyderma</i>	14111 ± 124	16800 - 15900
340-341	<i>N. pachyderma</i>	15131 ± 142	17800 - 17100
450-451	<i>N. pachyderma</i>	15112 ± 151	18100 - 17400
584-585	<i>G. bulloides</i>	16893 ± 203	20200 - 19100
686-687	<i>G. bulloides</i>	20432 ± 202	24200 - 23100

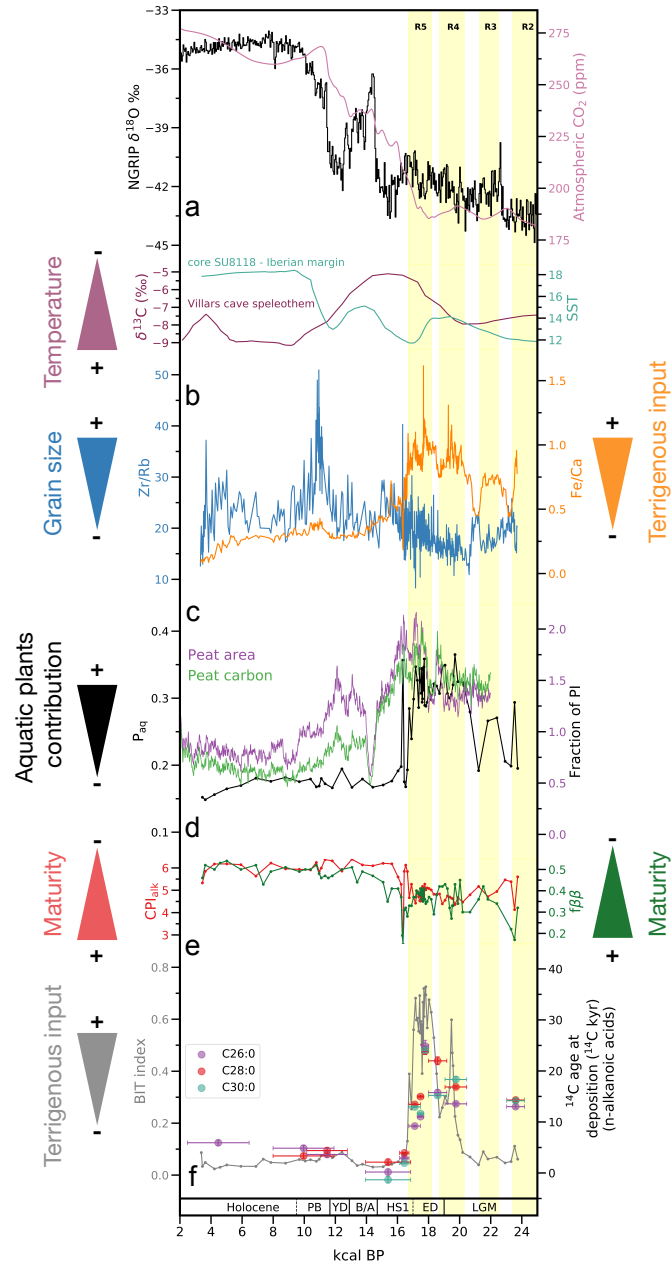


Figure 2. **a:** NGRIP $\delta^{18}\text{O}$ (Andersen et al., 2004) and atmospheric CO_2 (Köhler et al., 2017) records. **b:** Sea surface temperatures in the Northeast Atlantic Ocean (Bard et al., 2000) and $\delta^{13}\text{C}$ values from speleothems in Western Europe (Wainer et al., 2011). The data were smoothed to eliminate very high-frequency components. **c:** Zr/Rb and Fe/Ca elemental ratios from XRF data. **d:** Peatland area (purple) and carbon (green) in Europe as a fraction of pre-industrial (PI) values (0.231 Mkm^2 and 19.6 GtC) (Müller and Joos, 2020) and the P_{aq} index record. **e:** $f\beta\beta$ and CPI_{alk} records. **f:** Pre-depositional ^{14}C ages of n -alkanoic acids from core GeoB23302-2 and BIT index record. Yellow bands mark major flooding events of the Channel River (Toucanne et al., 2015).

Table 2. Carbon stable isotope ($\delta^{13}\text{C}$) values of bulk sediment samples from core GeoB23302-2.

Depth (cm)	Age (^{14}C yr)	Uncertainty (^{14}C yr)	$\delta^{13}\text{C}$ (‰)
30-33	4467	1988	-22.25
90-93	9957	1960	-22.22
140-143	11471	1304	-22.07
202-205	15397	1456	-23.37
247-250	16441	301	-23.88
302-305	17108	373	-25.72
350-353	17482	194	-25.93
451-454	17778	236	-25.83
510-513	18585	591	-25.09
590-593	19761	699	-24.44
680-683	23604	576	-23.23

230 4 Discussion

4.1 Source of the OM in the sedimentary record

Our results corroborate the previous findings of Ménot et al. (2006), showing a notable increase in the influx of terrigenous OM in the Bay of Biscay during the last deglacial period. Between ca. 20.6 and 15 kcal BP, the values of the Zr/Rb ratio reflect the deposition of coarse-grained sediments at the core location, which may be associated with enhanced fluvial activity (Wang et al., 2011). A period of relatively high Fe/Ca values (ca. 21 - 16.4 kcal BP) is indicative of a greater influx of sediment from land (Figure 2c). This is consistent with a period of elevated terrestrial contribution to the bulk OM present in the sediment, from approximately 20.5 to 16.5 kcal BP, except for a sudden decrease at approximately 19 kcal BP, as revealed by the BIT index (see e.g., Hopmans et al., 2004; Herfort et al., 2006; Kim et al., 2006; Schouten et al., 2013; Grotheer et al., 2020) (Figure 2f). These Fe/Ca and BIT patterns are also recorded in core MD95 2002 (see Figures 3 and 4 in the Supplementary Material; Toucanne et al., 2015; Ménot et al., 2006, respectively) and a similar pattern of marked Fe/Ca peaks, sometimes associated with peaks in OM content, during Heinrich events and much lower values throughout the Holocene has been observed at other sites (Jennerjahn et al., 2004; Lebreiro et al., 2009; Zhang et al., 2015; Crivellari et al., 2018).

Beyond identifying the presence of terrestrial OM transported to the Bay of Biscay via the Channel River during the LGM-Holocene transition, the comprehensive analysis of elemental, geochemical, and isotopic proxies presented here provides insights into the potential sources of this terrigenous OM. Values for the P_{aq} proxy point to a major contribution of OM from aquatic plants between approximately 20.2 and 17.2 kcal BP, suggesting the presence of OM sourced from wetland vegetation (Figure 2d). Our CPI_{alk} record reflects the degree of degradation the sedimentary OM has undergone in its previous terrestrial reservoir or during transportation (cf. Bröder et al., 2018). During the peak of terrigenous deposition, the signal of more mature OM fluvially transported to the continental slope is detected in our CPI_{alk} and $f\beta\beta$ records, which reach relatively low val-

250 ues when compared to the Holocene (Figure 2e). The presence of petrogenic, i.e., thermally-mature, material (Farrington and Tripp, 1977; Jeng, 2006) is another factor to consider when interpreting these records. Nonetheless, throughout the archive, the CPI_{alk} values remain above the diagnostic value of petrogenic material (ca. 1) reported by Bray and Evans (1961). Additionally, in contrast with the results of Meyer et al. (2019) for the Bering Sea, in the present study the $f\beta\beta$ proxy is not indicative of petrogenic material in the sediment (see the Supplementary Material). This is because the values do not decrease in response
255 to diagenetic transformations but rather due to enhanced inputs of the $C31\alpha\beta R$ hopane, which is abundant in peat (Inglis et al., 2018).

The compound-specific ^{14}C results disclose that the analyzed terrigenous biomarkers are ancient and pre-aged, indicating that they are not contemporaneous with sediment deposition but rather older (Figure 2f). Despite the large variability of OM residence time in permafrost soils, the pre-depositional ages of some of the compounds present in core GeoB23302-2 are
260 considerably greater than those previously attributed to permafrost-derived OM at other sites and at different timescales (e.g., Gustafsson et al., 2011; Winterfeld et al., 2018). Although petrogenic contributions are commonly thought to be devoid of *n*-alkanoic acids, this assumption does not always hold (Kvenvolden, 1966) and the erosion of organic-rich sedimentary rocks can supply fossil OM to the ocean, thereby depleting the ^{14}C compound-specific signal in the sediment (e.g., Raymond et al., 2004; Copard et al., 2007; Wu et al., 2022, and references therein). However, the OM present in core GeoB23302-2 presents $\delta^{13}C$
265 values in the range from -25.9 to -22.3‰, heavier than the average value of $\delta^{13}C = -29.4$ ‰ displayed by organic-rich rocks in the region (e.g., Zhao et al., 2022). These values are rather comparable to those observed in peat, corroborating the results of the CPI_{alk} and $f\beta\beta$ proxies and pointing to a pre-aged immature source such as ancient peat. The pre-depositional ages observed during the peak of OM deposition likely result from a ^{14}C reservoir effect, which is caused by radioactive decay and a lack of exchange with the atmosphere (Stuiver and Polach, 1977). This effect occurs as the OM is stored in its source reservoir before
270 eventual erosion and transportation to the core location. Mechanisms such as deposition-resuspension loops on the continental slope could be invoked to explain pre-aged *n*-alkanoic acids during the most recent part of our record (Kusch et al., 2021, and references therein). To summarize, our results strongly support previous findings describing a massive remobilization of terrestrial C from the European continent to the North Atlantic Ocean during the last deglaciation, with notable peaks at ca. 19.5 and between approximately 19 and 17 kcal BP (Ménot et al., 2006). In addition, the set of proxies applied in the present
275 study allows us to go further and suggest peat-derived material as a major source of OM to the Bay of Biscay during the last deglaciation.

4.2 Landscape development and OM remobilization mechanisms

Wetlands are dynamic ecosystems that fix CO_2 from the atmosphere, store C and contribute to the C cycle through various processes, including the decomposition of OM that releases CO_2 (Mitra et al., 2003). Therefore, the establishment of wetlands
280 in the study region towards the end of the LGM and during the last deglaciation (Figure 2d), combined with permafrost distribution data that imply gradual permafrost decomposition (e.g., Vandenberghe and Pissart, 1993; Levvasseur et al., 2011; Vandenberghe et al., 2012; Schaefer et al., 2014; Vandenberghe et al., 2014) and records of atmospheric CO_2 concentration (Köhler et al., 2017), suggests the need to investigate thawing permafrost as a possible source of OM to the deposition site. Al-

though some of the peatlands formed during the Eemian period were buried by glaciers and mineral sediments, Weichselian ice
285 sheets were not as extensive as the ones from the Saalian and some deposits remained uncovered (e.g., in Northern Germany, on
the cliff of the Elbe River; Ehlers et al., 2011). Peat deposits formed during the last interglacial occur widely across the studied
region (Turner, 2000), from Belgium (e.g., De Moor, 1983) and the Netherlands (e.g., Schokker et al., 2004) to Poland (e.g.,
Woronko et al., 2018), through Germany (e.g., Börner et al., 2018; Grube and Usinger, 2017) and Denmark (e.g., Christiansen,
1998). Although the environmental conditions of the last glaciation were unfavorable for the development of peatlands, factors
290 such as the formation of permafrost in Europe resulted in the long-term preservation of OM from older periods (e.g., frozen
peat OM) (Treat et al., 2019). However, during the last deglaciation, the thawing of permafrost and the presence of meltwater
streams may have contributed to the erosion of these peats. We propose that Eemian peatlands represent the primary source of
fossil biomarkers transported to the Bay of Biscay, with processes such as thermal and physical erosion of these deposits (see
e.g., Sidorchuk et al., 2009, 2011) leading to pre-aged material reaching the final burial site.

295 In Northwest and Central Europe, continuous permafrost prevailed at approximately 27-17 kcal BP (Vandenberghe and
Pissart, 1993), with the deposits likely degrading and shrinking due to the warming observed at the end of the LGM. For
instance, in the Netherlands, there has been evidence of widespread permafrost degradation between 22 and 21 kcal BP (Van
Huissteden et al., 2000), with continuous permafrost in the Dutch coversand region completely disappearing after 20 kcal
BP (Bateman and Van Huissteden, 1999). This episode is an example of permafrost thawing that may have contributed to
300 wetland development between ca. 21 and 16 kcal BP as recorded in our P_{aq} record (Figure 2d). Between 17 and 15 kcal BP,
permafrost zones in the study region were restricted to areas near the retreating ice-sheets (Renssen and Vandenberghe, 2003,
and references therein). Afterwards, apart from a short later period of discontinuous permafrost (ca. 10.9 - 10.5 kcal BP) that
has also been reported for Northwest and Central Europe (Vandenberghe and Pissart, 1993), there is evidence of the presence
of permafrost in this region during the Younger Dryas (e.g., Isarin, 1997; Petera-Zganiacz and Dzeduszyńska, 2017).

305 The erosion of European permafrost and peatland deposits by glacial meltwater is a mechanism likely to have exported
OM to the ocean. The decay of the European ice sheets and glaciers at the onset of the last deglaciation (e.g., Marks, 2002;
Rinterknecht et al., 2006; Ó Cofaigh and Evans, 2007; Ballantyne and Ó Cofaigh, 2017; Patton et al., 2017) contributed to
strengthening the Channel River discharge into the Bay of Biscay (Antoine et al., 2003; Bourillet et al., 2003) and it has
been proposed that this was the main mechanism controlling the river activity during this time period (Toucanne et al., 2009).
310 Deglacial pulses of meltwater emanating from the BIIS (at 22 and 18.6 kcal BP) and the FIS (starting around 19 kcal BP)
(Bowen et al., 2002; Rinterknecht et al., 2006) were routed to the North Atlantic via the Channel River. In this way, the
activity of the river responded to changes in the European ice masses, being particularly influenced by the dynamics of the FIS
(Toucanne et al., 2010).

Although subglacial meltwater can flow through permeable sediments as groundwater, the presence of frozen ground with
315 reduced hydraulic transmissivity, i.e., permafrost, hinders this process (Piotrowski, 1997). This leads to trapped pressurized
water accumulating underneath ice sheets and eventually draining during catastrophic events. As the climate warmed and the
ice sheets retreated and/or permafrost decayed, bursts of subglacial meltwater were released, carving glacial features known
as tunnel valleys in the ground and discharging large amounts of eroded material into rivers (Piotrowski, 1994, 1999; Kirkham

et al., 2022, and references therein). Subglacial channels from major Pleistocene glaciations are still present today in Europe
320 and serve as evidence of this phenomenon (e.g., Piotrowski, 1999; Piotrowski et al., 1999). Meltwater streams from the FIS
discharged through the Elbe River and provoked several flooding events of the Channel River (Mangerud et al., 2004; Toucanne
et al., 2015), with remarkable episodes (R2-R5) recorded as peaks in the ratios Ti/Ca and Fe/Ca of both the GeoB23302-2
and the MD95 2002 archives (Supplementary Figure 3). Floods R2-R5 were most likely associated with enhanced processes
of erosion and sediment export in the catchment (see e.g., Bogen and Bønsnes, 2003) and the intensified freshwater influx,
325 resulting from riverine discharge due to a mixture of precipitation and glacial meltwaters, is reflected in the terrestrially-
sourced OM signal shown by our BIT index record, which corroborates that reported for core MD95 2002 (Ménot et al., 2006)
(Supplementary Figure 4). Furthermore, the process of post-glacial sea-level rise may have played a role in the erosion of
coastal permafrost deposits, potentially serving as an additional pathway for the transport of OM to the ocean (e.g., Meyer
et al., 2019).

330 The remobilization of OM from land to ocean is largely mediated by rivers, with factors such as precipitation and temperature
being major regulators of fluvial C fluxes (Bauer et al., 2013, and references therein). Between 21 and 17 kcal BP, a temperature
rise (Figure 2a) observed in various Atlantic environmental records (e.g., Arz et al., 1999; Bard et al., 2000; Combourieu Nebout
et al., 2002; Pailler and Bard, 2002), marked a transition from cold and dry to warm and wet conditions in continental Europe.
For example, a gradual increase in the Northeast Atlantic SST starting at about 25 kcal BP and preceding the peak of terrigenous
335 deposition is recorded in core SU8118 (37°46'N, 10°11'W) (Bard et al., 2000). This same warming trend can be observed on
land, reflected in the $\delta^{13}\text{C}$ signature of a speleothem record from Western Europe (45°30'N, 0°50'E) (Wainer et al., 2011) and
starting roughly at the same time (Figure 2b). The speleothem timeseries is not high resolution and long-term trends may be in
fact punctuated with short-term oscillations. In any case, it is important to acknowledge that, although speleothem $\delta^{13}\text{C}$ values
can potentially serve as a proxy for temperature (see e.g., Lechleitner et al., 2021, and references therein), the correlation must
340 be interpreted with caution due to several other factors influencing C isotopic ratios in these archives (Fohlmeister et al., 2020).
Enhanced precipitation in response to warming led to increases in fluvial runoff and, due to widespread permafrost, increased
erosion and transport of sediment from land to the Channel River outlet (Ménot et al., 2006). After approximately 18 kcal
BP, as the climate warmed, the area occupied by peatlands in Europe increased (Müller and Joos, 2020). This is in agreement
with our P_{aq} index record, which indicates the re-establishment of formerly frozen wetlands, potentially including peat-rich
345 environments (Figure 2d).

Considering that the OM buried in marine sediment is only a relatively small part of the total OM entering rivers, which
is predominantly returned to the atmosphere as CO_2 (e.g., Aufdenkampe et al., 2011), the OM export to the Bay of Biscay
via the Channel River is likely to have been accompanied by the transfer of CO_2 and CH_4 to the atmosphere (e.g., Schneider
Von Deimling et al., 2015; Schuur et al., 2015; Bröder et al., 2018). It follows that our comprehensive analysis, encompassing
350 biomarkers, elemental proxies, and radiocarbon dating, consistently corroborates the hypothesis of permafrost thawing in
the Northern Hemisphere contributing to the observed perturbations in the atmospheric C reservoir (Köhler et al., 2014). This
essentially means that Northwest and Central Europe too, similar to other permafrost sites (Winterfeld et al., 2018; Meyer et al.,
2019), may have contributed to the deglacial rise in atmospheric CO_2 (Köhler et al., 2014; Marcott et al., 2014). However, it

is likely that the deglacial loss of European permafrost was offset by the subsequent accumulation of significant amounts of
355 C in permafrost-free soils and peatlands (Lindgren et al., 2018). Our elevated pre-depositional ages at ca. 17.5 kcal BP (up
to ca. 15 ¹⁴C kyr) may partly explain the steep drop in the ¹⁴C signature of atmospheric CO₂ during the period known as the
Mystery Interval (17.5 – 14.5 kyr BP) (see e.g., Broecker and Barker, 2007). In other words, this result implies that thawing
European permafrost combined with the deep ocean reservoir contributed ¹⁴C-depleted CO₂ to the atmosphere during this
period. However, our results show that the remobilization of C from this terrestrial pool started as early as ca. 20.2 kcal BP,
360 which considerably precedes estimates of large permafrost contributions to atmospheric CO₂ between 17.5 and 15 kyr BP
(Crichton et al., 2016). This suggests the need to investigate leads and lags in the permafrost carbon feedback.

After approximately 18 kcal BP, a re-routing of the Elbe-Weser system meant that FIS meltwater carrying ancient C was
being delivered to the Norwegian Channel (Toucanne et al., 2010, and references therein). After 17 kcal BP, sea-level rise
caused a shift of the shoreline, with the Bay of Biscay no longer being suitable to record terrestrial runoff during the Holocene
365 (Lambeck, 1997). This is reflected in the sudden drop observed in the BIT index record (Figure 2f). Notably, although our data
support what has been previously inferred for the study region (Ménot et al., 2006; Rostek and Bard, 2013; Soulet et al., 2013),
the distinct timing for the discharge peak observed in this study compared to other sites may imply different mechanisms of C
remobilization and these need to be further investigated. Indeed, factors such as the local hydrology and vegetation have been
shown to play a role in the accumulation and degradation pathways of permafrost-influenced peatlands (Hugelius et al., 2020,
370 and references therein).

Peat-forming wetlands remain an important source of terrestrial OM to the ocean and of CH₄ and CO₂ to the atmosphere,
with flux rates likely increasing due to current warming (Freeman et al., 2001; Hodgkins et al., 2014). In high northern lat-
itude wetlands, it has been shown that permafrost degradation leads to wetland shrinkage (Avis et al., 2011). In the tropics
the situation is also critical, with anthropogenic (Moore et al., 2013) and natural (Schefuß et al., 2016; Garcin et al., 2022)
375 factors contributing to the remobilization of pre-aged C from peatlands. Therefore, the release of large amounts of peat-derived
OM described here for deglacial Europe has analogues in the present day and may be useful to inform future projections of
permafrost peatland loss (e.g., Fewster et al., 2022), with our results advocating for the importance of better constraining the C
cycle in wetlands.

5 Conclusions

380 To reconcile the great pre-depositional ages observed here with geochemical data that do not hint towards highly-degraded
petrogenic material, we argue that the OM in core GeoB23302-2 is mostly derived from ancient continental peat deposits.
During the last interglacial, peatlands were established in the European landscape. These deposits were widely distributed
and were preserved in a frozen state throughout the last glaciation due to the widespread presence of permafrost. Over the
course of the last deglaciation, warming and episodes of ice-sheet retreat and associated flooding through the Channel River
385 resulted in the erosion of these permafrost deposits, enhancing the downstream transport of sediment and mobilising ancient
C to the core site. Our results indicate that during the period between 20.2 and 15.8 kcal BP, a substantial portion of the OM

transported to the Bay of Biscay originated from ancient European peatlands. After approximately 17 kcal BP, our core location was not suitable for recording terrigenous inputs via the Channel River. Instead, the Norwegian Channel may have become the primary recipient of fluvially-discharged permafrost-derived C. It is possible that the emission of greenhouse gases resulting from the degradation of formerly frozen OM in European permafrost contributed to the rapid rise of approximately 30 ppm in the atmospheric CO₂ concentration between 17.5 and 16 kcal BP. However, further investigation is needed to accurately quantify the rates and magnitudes of the processes responsible for this contribution. This study provides empirical evidence of a cycle of peat formation during warm periods and long-term storage under colder conditions. Owing to the size of the C pool involved, such a mechanism is likely to increase atmospheric greenhouse gas concentrations, with important implications for Earth's climate. In this context, our results will be useful to better constrain the role of ancient C mobilization and the permafrost carbon feedback in climate models.

Data availability. Data generated in this study are freely available at <https://doi.pangaea.de/10.1594/PANGAEA.954937>

Author contributions. GM designed the study. GM, KZ and HG collected the sediment core. Funding for the project was acquired by GM and EQA. EQA and WW conducted the laboratory analyses with the support of JH, HG, TG and TT. EQA, GM, JH, HG and WW analyzed the data. EQA wrote the paper and generated the figures. All authors provided feedback on the paper.

Competing interests. The authors declare that they have no conflict of interest.

Acknowledgements. This research was funded by the Alexander von Humboldt Foundation via a post-doctoral fellowship granted to EQA. Thanks are also due to the Brazilian National Council for Scientific and Technological Development (CNPq) for the support provided to EQA. HG was funded by the German Science Foundation within the Cluster of Excellence EXC 2077 “The Oceans Floor – Earth’s Uncharted Interface” (Project number 390741603). We thank Dr Enno Schefuß and Professor Kita Macario for helpful discussions that benefited this research. We are also grateful for the data provided by Dr Samuel Toucanne and Professor Fortunat Joos, and for the technical laboratory support offered by Elizabeth Bonk and Lea Phillips.

References

- Andersen, K. K., Azuma, N., Barnola, J. M., Bigler, M., Biscaye, P., Caillon, N., Chappellaz, J., Clausen, H. B., Dahl-Jensen, D., Fischer, H.,
410 Flückiger, J., Fritzsche, D., Fujii, Y., Goto-Azuma, K., Grønbold, K., Gundestrup, N. S., Hansson, M., Huber, C., Hvidberg, C. S., Johnsen,
S. J., Jonsell, U., Jouzel, J., Kipfstuhl, S., Landais, A., Leuenberger, M., Lorrain, R., Masson-Delmotte, V., Miller, H., Motoyama, H.,
Narita, H., Popp, T., Rasmussen, S. O., Raynaud, D., Rothlisberger, R., Ruth, U., Samyn, D., Schwander, J., Shoji, H., Siggard-Andersen,
M. L., Steffensen, J. P., Stocker, T., Sveinbjörnsdóttir, A. E., Svensson, A., Takata, M., Tison, J. L., Thorsteinsson, T., Watanabe, O.,
415 Wilhelms, F., and White, J. W.: High-resolution record of Northern Hemisphere climate extending into the last interglacial period, *Nature*,
431, 147–151, 2004.
- Antoine, P., Coutard, J. P., Gibbard, P., Hallegouet, B., Lautridou, J. P., and Ozouf, J. C.: The Pleistocene rivers of the English Channel
region, *Journal of Quaternary Science*, 18, 227–243, 2003.
- Arz, H. W., Pätzold, J., and Wefer, G.: Climatic changes during the last deglaciation recorded in sediment cores from the northeastern
Brazilian Continental Margin, *Geo-Marine Letters*, 19, 209–218, 1999.
- 420 Aufdenkampe, A. K., Mayorga, E., Raymond, P. A., Melack, J. M., Doney, S. C., Alin, S. R., Aalto, R. E., and Yoo, K.: Riverine coupling of
biogeochemical cycles between land, oceans, and atmosphere, *Frontiers in Ecology and the Environment*, 9, 53–60, 2011.
- Avis, C. A., Weaver, A. J., and Meissner, K. J.: Reduction in areal extent of high-latitude wetlands in response to permafrost thaw, *Nature
Geoscience*, 4, 444–448, 2011.
- Ballantyne, C. K. and Ó Cofaigh, C.: The Last Irish Ice Sheet: Extent and Chronology, in: *Advances in Irish Quaternary Studies*, pp. 101–149,
425 Atlantis Press, Paris, <https://doi.org/10.3318/ijes.2018.36.4>, 2017.
- Bard, E., Rostek, F., Turon, J. L., and Gendreau, S.: Hydrological impact of Heinrich events in the subtropical Northeast Atlantic, *Science*,
289, 1321–1324, 2000.
- Bateman, M. D. and Van Huissteden, J.: The timing of last-glacial periglacial and aeolian events, Twente, eastern Netherlands, *Journal of
Quaternary Science*, 14, 277–283, 1999.
- 430 Bauer, J. E., Cai, W. J., Raymond, P. A., Bianchi, T. S., Hopkinson, C. S., and Regnier, P. A.: The changing carbon cycle of the coastal ocean,
Nature, 504, 61–70, 2013.
- Bauska, T. K., Baggenstos, D., Brook, E. J., Mix, A. C., Marcott, S. A., Petrenko, V. V., Schaefer, H., Severinghaus, J. P., Lee, J. E., and
Thiemens, M. H.: Carbon isotopes characterize rapid changes in atmospheric carbon dioxide during the last deglaciation, *Proceedings of
the National Academy of Sciences of the United States of America*, 113, 3465–3470, 2016.
- 435 Bianchi, T. and Canuel, E.: *Chemical biomarkers in aquatic ecosystems*, Princeton University Press, 2011.
- Bogen, J. and Bønsnes, T. E.: Erosion and sediment transport in High Arctic rivers, Svalbard, *Polar Research*, 22, 175–189, 2003.
- Börner, A., Hrynowiecka, A., Stachowicz-Rybka, R., Niska, M., Moskal-del Hoyo, M., Kuznetsov, V., Maksimov, F., and Petrov, A.:
Palaeoecological investigations and ²³⁰Th/U dating of the Eemian Interglacial peat sequence from Neubrandenburg-Hinterste Mühle
(Mecklenburg-Western Pomerania, NE Germany), *Quaternary International*, 467, 62–78, 2018.
- 440 Bourillet, J. F., Reynaud, J. Y., Baltzer, A., and Zaragosi, S.: The 'Fleuve Manche': The submarine sedimentary features from the outer shelf
to the deep-sea fans, *Journal of Quaternary Science*, 18, 261–282, 2003.
- Bowen, D. Q., Phillips, F. M., McCabe, A. M., Knutz, P. C., and Sykes, G. A.: New data for the Last Glacial Maximum in Great Britain and
Ireland, *Quaternary Science Reviews*, 21, 89–101, 2002.

- Bray, E. E. and Evans, E. D.: Distribution of n-paraffins as a clue to recognition of source beds, *Geochimica et Cosmochimica Acta*, 22, 445 2–15, 1961.
- Bröder, L., Tesi, T., Andersson, A., Semiletov, I., and Gustafsson, Ö.: Bounding cross-shelf transport time and degradation in Siberian-Arctic land-ocean carbon transfer, *Nature Communications*, 9, 2018.
- Broecker, W. and Barker, S.: A 190‰ drop in atmosphere's $\Delta^{14}\text{C}$ during the "Mystery Interval" (17.5 to 14.5 kyr), *Earth and Planetary Science Letters*, 256, 90–99, 2007.
- 450 Bronk Ramsey, C.: Radiocarbon calibration and analysis of stratigraphy: the OxCal program, *Radiocarbon*, 37, 425–430, 1995.
- Bronk Ramsey, C.: Deposition models for chronological records, *Quaternary Science Reviews*, 27, 42–60, 2008.
- Bronk Ramsey, C.: Bayesian analysis of radiocarbon dates, *Radiocarbon*, 51, 337–360, 2009a.
- Bronk Ramsey, C.: Dealing with outliers and offsets in radiocarbon dating, *Radiocarbon*, 51, 1023–1045, 2009b.
- Bronk Ramsey, C. and Lee, S.: Recent and Planned Developments of the Program OxCal, *Radiocarbon*, 55, 720–730, 2013.
- 455 Christiansen, H. H.: Periglacial sediments in an Eemian-Weichselian succession at Emmerlev Klev, southwestern Jutland, Denmark, *Palaeogeography, Palaeoclimatology, Palaeoecology*, 138, 245–258, 1998.
- Ciais, P., Tagliabue, A., Cuntz, M., Bopp, L., Scholze, M., Hoffmann, G., Lourantou, A., Harrison, S. P., Prentice, I. C., Kelley, D. I., Koven, C., and Piao, S. L.: Large inert carbon pool in the terrestrial biosphere during the Last Glacial Maximum, *Nature Geoscience*, 5, 74–79, 2012.
- 460 Combourieu Nebout, N., Turon, J. L., Zahn, R., Capotondi, L., Londeix, L., and Pahnke, K.: Enhanced aridity and atmospheric high-pressure stability over the western Mediterranean during the North Atlantic cold events of the past 50 k.y, *Geology*, 30, 863–866, 2002.
- Copard, Y., Amiotte-Suchet, P., and Di-Giovanni, C.: Storage and release of fossil organic carbon related to weathering of sedimentary rocks, *Earth and Planetary Science Letters*, 258, 345–357, 2007.
- Crichton, K. A., Bouttes, N., Roche, D. M., Chappellaz, J., and Krinner, G.: Permafrost carbon as a missing link to explain CO₂ changes 465 during the last deglaciation, *Nature Geoscience*, 9, 683–686, 2016.
- Crivellari, S., Chiessi, C. M., Kuhnert, H., Häggi, C., da Costa Portilho-Ramos, R., Zeng, J. Y., Zhang, Y., Schefuß, E., Mollenhauer, G., Hefter, J., Alexandre, F., Sampaio, G., and Mulitza, S.: Increased Amazon freshwater discharge during late Heinrich Stadial 1, *Quaternary Science Reviews*, 181, 144–155, 2018.
- De Moor, G.: Cryogenic Structures in the Weichselian Deposits of Northern Belgium and their Significance, *Polarforschung*, 53, 79–86, 470 1983.
- Dickson, A. J., Leng, M. J., Maslin, M. A., and Röhl, U.: Oceanic, atmospheric and ice-sheet forcing of South East Atlantic Ocean productivity and South African monsoon intensity during MIS-12 to 10, *Quaternary Science Reviews*, 29, 3936–3947, <http://dx.doi.org/10.1016/j.quascirev.2010.09.014>, 2010.
- Dypvik, H. and Harris, N. B.: Geochemical facies analysis of fine-grained siliciclastics using Th/U, Zr/Rb and (Zr + Rb)/Sr ratios, *Chemical 475 Geology*, 181, 131–146, 2001.
- Eglinton, T. I., Aluwihare, L. I., Bauer, J. E., Druffel, E. R., and McNichol, A. P.: Gas chromatographic isolation of individual compounds from complex matrices for radiocarbon dating, *Analytical Chemistry*, 68, 904–912, 1996.
- Ehlers, J., Grube, A., Stephan, H. J., and Wansa, S.: Pleistocene glaciations of North Germany-New results, *Developments in Quaternary Science*, 15, 149–162, 2011.
- 480 Fairbanks, R. G.: A 17,000-year glacio-eustatic sea level record: influence of glacial melting rates on the Younger Dryas event and deep-ocean circulation, *Nature*, 342, 637–642, 1989.

- Farrington, J. W. and Tripp, B. W.: Hydrocarbons in western North Atlantic surface sediments, *Geochimica et Cosmochimica Acta*, 41, 1627–1641, 1977.
- 485 Feurdean, A., Grindean, R., Florescu, G., Tantău, I., Niedermeyer, E. M., Diaconu, A. C., Hutchinson, S. M., Nielsen, A. B., Sava, T., Panait, A., Braun, M., and Hickler, T.: The transformation of the forest steppe in the lower Danube Plain of southeastern Europe: 6000 years of vegetation and land use dynamics, *Biogeosciences*, 18, 1081–1103, 2021.
- Fewster, R. E., Morris, P. J., Ivanovic, R. F., Swindles, G. T., Peregón, A. M., and Smith, C. J.: Imminent loss of climate space for permafrost peatlands in Europe and Western Siberia, *Nature Climate Change*, 12, 373–379, 2022.
- 490 Ficken, K. J., Li, B., Swain, D. L., and Eglinton, G.: An n-alkane proxy for the sedimentary input of submerged/floating freshwater aquatic macrophytes, *Organic Geochemistry*, 31, 745–749, 2000.
- Fohlmeister, J., Voarintsoa, N. R. G., Lechleitner, F. A., Boyd, M., Brandtstätter, S., Jacobson, M. J., and Oster, J. L.: Main controls on the stable carbon isotope composition of speleothems, *Geochimica et Cosmochimica Acta*, 279, 67–87, 2020.
- Freeman, C., Evans, C., and Monteih, D.: Export of organic carbon from peat soils, *Nature*, 412, 785, 2001.
- Garcin, Y., Schefuß, E., Dargie, G. C., Hawthorne, D., Lawson, I., Sebg, D., Biddulph, G., Crezee, B., Bocko, Y., Ifo, S., Wenina, Y., 495 Mbemba, M., Ewango, C., Emba, O., Bola, P., Tabu, J., Tyrrell, G., Young, DM, Gassier, G., Girkin, N., Vane, C., Adatte, T., Baird, A., Boom, A., Gulliver, P., Morris, P., Page, S., Sjögersten, S., and Lewis, S.: Hydroclimatic vulnerability of peat carbon in the central Congo Basin, *Nature*, 612, 277–282, 2022.
- Gibbard, P. L.: The history of the great northwest European rivers during the past three million years, *Philosophical Transactions of the Royal Society of London. B, Biological Sciences*, 318, 559–602, 1988.
- 500 Grotheer, H., Meyer, V., Riedel, T., Pfalz, G., Mathieu, L., Hefter, J., Gentz, T., Lantuit, H., Mollenhauer, G., and Fritz, M.: Burial and Origin of Permafrost-Derived Carbon in the Nearshore Zone of the Southern Canadian Beaufort Sea, *Geophysical Research Letters*, 47, 2020.
- Grube, A. and Usinger, H.: Spring fed raised peat hummocks with tufa deposits at the Farbeberg hills (Northwest-Germany): Structure, genesis and paleoclimatic conclusions (Eemian, Holocene), *E and G Quaternary Science Journal*, 66, 14–31, 2017.
- Gustafsson, Ö., Van Dongen, B. E., Vonk, J. E., Dudarev, O. V., and Semiletov, I. P.: Widespread release of old carbon across the Siberian 505 Arctic echoed by its large rivers, *Biogeosciences*, 8, 1737–1743, 2011.
- He, D., Nemiah Ladd, S., Saunders, C. J., Mead, R. N., and Jaffé, R.: Distribution of n-alkanes and their $\delta^2\text{H}$ and $\delta^{13}\text{C}$ values in typical plants along a terrestrial-coastal-oceanic gradient, *Geochimica et Cosmochimica Acta*, 281, 31–52, 2020.
- Heaton, T. J., Köhler, P., Butzin, M., Bard, E., Reimer, R. W., Austin, W. E., Bronk Ramsey, C., Grootes, P. M., Hughen, K. A., Kromer, B., Reimer, P. J., Adkins, J., Burke, A., Cook, M. S., Olsen, J., and Skinner, L. C.: Marine20 - The Marine Radiocarbon Age Calibration 510 Curve (0-55,000 cal BP), *Radiocarbon*, 62, 779–820, 2020.
- Heaton, T. J., Bard, E., Bronk Ramsey, C., Butzin, M., Hatté, C., Hughen, K. A., Köhler, P., and Reimer, P. J.: a Response To Community Questions on the Marine20 Radiocarbon Age Calibration Curve: Marine Reservoir Ages and the Calibration of ^{14}C Samples From the Oceans, *Radiocarbon*, 65, 247–273, 2023.
- Hefter, J.: Analysis of Alkenone Unsaturation Indices with Fast Gas Chromatography/Time-of-Flight Mass Spectrometry, *Analytical Chemistry*, 80, 2161–2170, 2008.
- 515 Herfort, L., Schouten, S., Boon, J. P., Woltering, M., Baas, M., Weijers, J. W., and Sinninghe Damsté, J. S.: Characterization of transport and deposition of terrestrial organic matter in the southern North Sea using the BIT index, *Limnology and Oceanography*, 51, 2196–2205, 2006.

- Hodgkins, S. B., Tfaily, M. M., McCalley, C. K., Logan, T. A., Crill, P. M., Saleska, S. R., Rich, V. I., and Chanton, J. P.: Changes in peat chemistry associated with permafrost thaw increase greenhouse gas production, *Proceedings of the National Academy of Sciences of the United States of America*, 111, 5819–5824, <https://doi.org/10.1073/pnas.1314641111>, 2014.
- Hopmans, E. C., Weijers, J. W., Schefuß, E., Herfort, L., Sinninghe Damsté, J. S., and Schouten, S.: A novel proxy for terrestrial organic matter in sediments based on branched and isoprenoid tetraether lipids, *Earth and Planetary Science Letters*, 224, 107–116, 2004.
- Hopmans, E. C., Schouten, S., and Sinninghe Damsté, J. S.: The effect of improved chromatography on GDGT-based palaeoproxies, *Organic Geochemistry*, 93, 1–6, 2016.
- Hugelius, G., Strauss, J., Zubrzycki, S., Harden, J. W., Schuur, E. A., Ping, C. L., Schirrmeister, L., Grosse, G., Michaelson, G. J., Koven, C. D., O'Donnell, J. A., Elberling, B., Mishra, U., Camill, P., Yu, Z., Palmtag, J., and Kuhry, P.: Estimated stocks of circumpolar permafrost carbon with quantified uncertainty ranges and identified data gaps, *Biogeosciences*, 11, 6573–6593, 2014.
- Hugelius, G., Loisel, J., Chadburn, S., Jackson, R. B., Jones, M., MacDonald, G., Marushchak, M., Olefeldt, D., Packalen, M., Siewert, M. B., Treat, C., Turetsky, M., Voigt, C., and Yu, Z.: Large stocks of peatland carbon and nitrogen are vulnerable to permafrost thaw, *Proceedings of the National Academy of Sciences of the United States of America*, 117, 20438–20446, 2020.
- Inglis, G. N., Naafs, B. D. A., Zheng, Y., McClymont, E. L., Evershed, R. P., and Pancost, R. D.: Distributions of geohopanooids in peat: Implications for the use of hopanoid-based proxies in natural archives, *Geochimica et Cosmochimica Acta*, 224, 249–261, <https://doi.org/2017.12.029>, 2018.
- Isarin, R. F.: Permafrost distribution and temperatures in Europe during the Younger Dryas, *Permafrost and Periglacial Processes*, 8, 313–333, 1997.
- Itambi, A. C., Von Dobeneck, T., Mulitza, S., Bickert, T., and Heslop, D.: Millennial-scale northwest African droughts related to Heinrich events and Dansgaard-Oeschger cycles: Evidence in marine sediments from offshore Senegal, *Paleoceanography*, 24, 1–16, 2009.
- Jeng, W. L.: Higher plant n-alkane average chain length as an indicator of petrogenic hydrocarbon contamination in marine sediments, *Marine Chemistry*, 102, 242–251, 2006.
- Jennerjahn, T. C., Ittekkot, V., Arz, H. W., Behling, H., Pätzold, J., and Wefer, G.: Asynchronous terrestrial and marine signals of climate change during Heinrich events, *Science*, 306, 2236–2239, 2004.
- Keskitalo, K., Tesi, T., Bröder, L., Andersson, A., Pearce, C., Sköld, M., Semiletov, I. P., Dudarev, O. V., and Gustafsson, Ö.: Sources and characteristics of terrestrial carbon in Holocene-scale sediments of the East Siberian Sea, *Climate of the Past*, 13, 1213–1226, 2017.
- Kim, J. H., Schouten, S., Bonnin, J., Buscail, R., Ludwig, W., Sinninghe Damsté, J. S., and Bourrin, F.: Origin and distribution of terrestrial organic matter in the NW Mediterranean (Gulf of Lions): Exploring the newly developed BIT index, *Geochemistry, Geophysics, Geosystems*, 7, 2006.
- Kirkham, J. D., Hogan, K. A., Larter, R. D., Arnold, N. S., Ely, J. C., Clark, C. D., Self, E., Games, K., Huuse, M., Stewart, M. A., Ottesen, D., and Dowdeswell, J. A.: Tunnel valley formation beneath deglaciating mid-latitude ice sheets : Observations and modelling, *Quaternary Science Reviews*, p. 107680, 2022.
- Köhler, P., Knorr, G., and Bard, E.: Permafrost thawing as a possible source of abrupt carbon release at the onset of the Bølling/Allerød, *Nature Communications*, 5, 2014.
- Köhler, P., Nehrbass-Ahles, C., Schmitt, J., Stocker, T. F., and Fischer, H.: A 156 kyr smoothed history of the atmospheric greenhouse gases CO₂, CH₄ and NO₂ and their radiative forcing, *Earth System Science Data*, 9, 363–387, 2017.
- Koppes, M. and Hallet, B.: Erosion rates during rapid deglaciation in Icy Bay, Alaska, *Journal of Geophysical Research: Earth Surface*, 111, 1–11, 2006.

- Koppes, M. N. and Hallet, B.: Influence of rapid glacial retreat on the rate of erosion by tidewater glaciers, *Geology*, 30, 47–50, 2002.
- Kusch, S., Rethemeyer, J., Schefuß, E., and Mollenhauer, G.: Controls on the age of vascular plant biomarkers in Black Sea sediments, *Geochimica et Cosmochimica Acta*, 74, 7031–7047, 2010.
- 560 Kusch, S., Mollenhauer, G., Willmes, C., Hefter, J., Eglinton, T. I., and Galy, V.: Controls on the age of plant waxes in marine sediments – A global synthesis, *Organic Geochemistry*, 157, 2021.
- Kvenvolden, K. A.: Molecular Distributions of Normal Fatty Acids and Paraffins in Some Lower Cretaceous Sediments, *Nature*, pp. 573–577, 1966.
- Kylander, M. E., Ampel, L., Wohlfarth, B., and Veres, D.: High-resolution X-ray fluorescence core scanning analysis of Les Echets (France) 565 sedimentary sequence: New insights from chemical proxies, *Journal of Quaternary Science*, 26, 109–117, 2011.
- Lambeck, K.: Sea-level change along the French Atlantic and Channel coasts since the time of the Last Glacial Maximum, *Palaeogeography, Palaeoclimatology, Palaeoecology*, 129, 1–22, 1997.
- Lambeck, K., Rouby, H., Purcell, A., Sun, Y., and Sambridge, M.: Sea level and global ice volumes from the Last Glacial Maximum to the Holocene, *Proceedings of the National Academy of Sciences of the United States of America*, 111, 15 296–15 303, 2014.
- 570 Lebreiro, S. M., Voelker, A. H., Vizcaino, A., Abrantes, F. G., Alt-Epping, U., Jung, S., Thouveny, N., and Gràcia, E.: Sediment instability on the Portuguese continental margin under abrupt glacial climate changes (last 60 kyr), *Quaternary Science Reviews*, 28, 3211–3223, 2009.
- Lechleitner, F. A., Day, C. C., Kost, O., Wilhelm, M., Haghipour, N., Henderson, G. M., and Stoll, H. M.: Stalagmite carbon isotopes suggest deglacial increase in soil respiration in western Europe driven by temperature change, *Climate of the Past*, 17, 1903–1918, 2021.
- Levvasseur, G., Vrac, M., Roche, D. M., Paillard, D., Martin, A., and Vandenberghe, J.: Present and LGM permafrost from climate simula- 575 tions: Contribution of statistical downscaling, *Climate of the Past*, 7, 1225–1246, 2011.
- Lindgren, A., Hugelius, G., and Kuhry, P.: Extensive loss of past permafrost carbon but a net accumulation into present-day soils, *Nature*, 560, 219–222, 2018.
- Liu, X.-l., Lipp, J. S., Simpson, J. H., Lin, Y.-s., Summons, R. E., and Hinrichs, K.-u.: Mono- and dihydroxyl glycerol dibiphytanyl glycerol tetraethers in marine sediments : Identification of both core and intact polar lipid forms, *Geochimica et Cosmochimica Acta*, 89, 102–115, 580 2012.
- Mangerud, J., Jakobsson, M., Alexanderson, H., Astakhov, V., Clarke, G. K., Henriksen, M., Hjort, C., Krinner, G., Lunkka, J. P., Möller, P., Murray, A., Nikolskaya, O., Saarnisto, M., and Svendsen, J. I.: Ice-dammed lakes and rerouting of the drainage of northern Eurasia during the Last Glaciation, *Quaternary Science Reviews*, 23, 1313–1332, 2004.
- Marcott, S. A., Bauska, T. K., Buizert, C., Steig, E. J., Rosen, J. L., Cuffey, K. M., Fudge, T. J., Severinghaus, J. P., Ahn, J., Kalk, M. L., 585 McConnell, J. R., Sowers, T., Taylor, K. C., White, J. W., and Brook, E. J.: Centennial-scale changes in the global carbon cycle during the last deglaciation, *Nature*, 514, 616–619, 2014.
- Marks, L.: Last Glacial Maximum in Poland, *Quaternary Science Reviews*, 21, 103–110, 2002.
- Martens, J., Wild, B., Pearce, C., Tesi, T., Andersson, A., Bröder, L., O'Regan, M., Jakobsson, M., Sköld, M., Gemery, L., Cronin, T. M., Semiletov, I., Dudarev, O. V., and Gustafsson, Ö.: Remobilization of Old Permafrost Carbon to Chukchi Sea Sediments During the End 590 of the Last Deglaciation, *Global Biogeochemical Cycles*, 33, 2–14, 2019.
- Martens, J., Wild, B., Muschitiello, F., O'Regan, M., Jakobsson, M., Semiletov, I., Dudarev, O. V., and Gustafsson, Ö.: Remobilization of dormant carbon from Siberian-Arctic permafrost during three past warming events, *Science Advances*, 6, 2020.
- Marzi, R., Torkelson, B. E., and Olson, R. K.: A revised carbon preference index, *Organic Geochemistry*, 20, 1303–1306, 1993.

- Ménot, G., Bard, E., Rostek, F., Weijers, J. W. H., Hopmans, E. C., Schouten, S., and Damste, J. S. S.: Early Reactivation of European Rivers
595 During the Last Deglaciation, *Science*, 313, 1623–1625, 2006.
- Meyer, V. D., Hefter, J., Köhler, P., Tiedemann, R., Gersonde, R., Wacker, L., and Mollenhauer, G.: Permafrost-carbon mobilization in
Beringia caused by deglacial meltwater runoff, sea-level rise and warming, *Environmental Research Letters*, 14, 2019.
- Meyers, P. A. and Ishiwatari, R.: Lacustrine organic geochemistry-an overview of indicators of organic matter sources and diagenesis in lake
sediments, *Organic Geochemistry*, 20, 867–900, 1993.
- 600 Mitra, S., Wassmann, R., and Vlek, P. L. G.: Global inventory of wetlands and their role in the carbon cycle, ZEF Discussion Paper on
Development Policy, Bonn, p. 57, 2003.
- Mollenhauer, G., Grotheer, H., Gentz, T., Bonk, E., and Hefter, J.: Standard operation procedures and performance of the MICADAS radio-
carbon laboratory at Alfred Wegener Institute (AWI), Germany, *Nuclear Instruments and Methods in Physics Research, Section B: Beam
Interactions with Materials and Atoms*, 496, 45–51, <https://doi.org/10.1016/j.nimb.2021.03.016>, 2021.
- 605 Moore, S., Evans, C. D., Page, S. E., Garnett, M. H., Jones, T. G., Freeman, C., Hooijer, A., Wiltshire, A. J., Limin, S. H.,
and Gauci, V.: Deep instability of deforested tropical peatlands revealed by fluvial organic carbon fluxes, *Nature*, 493, 660–663,
<https://doi.org/10.1038/nature11818>, 2013.
- Müller, J. and Joos, F.: Global peatland area and carbon dynamics from the Last Glacial Maximum to the present – A process-based model
investigation, *Biogeosciences*, 17, 5285–5308, 2020.
- 610 Nichols, J. E., Booth, R. K., Jackson, S. T., Pendall, E. G., and Huang, Y.: Paleohydrologic reconstruction based on n-alkane distributions in
ombrotrophic peat, *Organic Geochemistry*, 37, 1505–1513, 2006.
- Nieuwenhuize, J., Maas, Y., and Middelburg, J.: Rapid Analysis of Organic Carbon.Pdf, *Marine Chemistry*, 45, 217–224, 1994.
- Ó Cofaigh, C. and Evans, D. J.: Radiocarbon constraints on the age of the maximum advance of the British-Irish Ice Sheet in the Celtic Sea,
Quaternary Science Reviews, 26, 1197–1203, 2007.
- 615 Pailler, D. and Bard, E.: High frequency palaeoceanographic changes during the past 140 000 yr recorded by the organic matter in sediments
of the Iberian Margin, *Palaeogeography, Palaeoclimatology, Palaeoecology*, 181, 431–452, 2002.
- Patton, H., Hubbard, A., Andreassen, K., Auriac, A., Whitehouse, P. L., Stroeve, A. P., Shackleton, C., Winsborrow, M., Heyman, J., and
Hall, A. M.: Deglaciation of the Eurasian ice sheet complex, *Quaternary Science Reviews*, 169, 148–172, 2017.
- Perez, L., García-Rodríguez, F., and Hanebuth, T. J.: Variability in terrigenous sediment supply offshore of the Río de la Plata (Uruguay)
620 recording the continental climatic history over the past 1200 years, *Climate of the Past*, 12, 623–634, 2016.
- Petera-Zganiacz, J. and Dzieduszyńska, D. A.: Palaeoenvironmental Proxies for Permafrost Presence During the Younger Dryas, Central
Poland, *Permafrost and Periglacial Processes*, 28, 726–740, 2017.
- Piotrowski, J. A.: Tunnel-valley formation in northwest Germany-geology, mechanisms of formation and subglacial bed conditions for the
Bornhöved tunnel valley, *Sedimentary Geology*, 89, 107–141, 1994.
- 625 Piotrowski, J. A.: Subglacial groundwater flow during the last deglaciation in northwestern Germany, *Sedimentary Geology*, 111, 217–224,
1997.
- Piotrowski, J. A.: Channelized subglacial drainage under soft-bedded ice sheets: Evidence from small N-channels in Central European
Lowland, *Geological Quarterly*, 43, 153–162, 1999.
- Piotrowski, J. A., Geletneky, J., and Vater, R.: Soft-bedded subglacial meltwater channel from the Welzow-Sud open-cast lignite mine, Lower
630 Lusatia, eastern Germany, *Boreas*, 28, 363–374, 1999.

- Raymond, P. A., Bauer, J. E., Caraco, N. F., Cole, J. J., Longworth, B., and Petsch, S. T.: Controls on the variability of organic matter and dissolved inorganic carbon ages in northeast US rivers, *Marine Chemistry*, 92, 353–366, 2004.
- Reimer, P. J., Austin, W. E., Bard, E., Bayliss, A., Blackwell, P. G., Bronk Ramsey, C., Butzin, M., Cheng, H., Edwards, R. L., Friedrich, M., Grootes, P. M., Guilderson, T. P., Hajdas, I., Heaton, T. J., Hogg, A. G., Hughen, K. A., Kromer, B., Manning, S. W., Muscheler, R., Palmer, J. G., Pearson, C., Van Der Plicht, J., Reimer, R. W., Richards, D. A., Scott, E. M., Southon, J. R., Turney, C. S., Wacker, L., Adolphi, F., Büntgen, U., Capano, M., Fahrni, S. M., Fogtmann-Schulz, A., Friedrich, R., Köhler, P., Kudsk, S., Miyake, F., Olsen, J., Reinig, F., Sakamoto, M., Sookdeo, A., and Talamo, S.: The IntCal20 Northern Hemisphere Radiocarbon Age Calibration Curve (0–55 cal kBP), *Radiocarbon*, 62, 725–757, 2020.
- 635 Renssen, H. and Vandenberghe, J.: Investigation of the relationship between permafrost distribution in NW Europe and extensive winter sea-ice cover in the North Atlantic Ocean during the cold phases of the Last Glaciation, *Quaternary Science Reviews*, 22, 209–223, 2003.
- 640 Rinterknecht, V. R., Clark, P. U., Raisbeck, G. M., Yiou, F., Bitinas, A., Brook, E. J., Marks, L., Zelcs, V., Lunkka, J. P., Pavlovskaya, I. E., Piotrowski, J. A., and Raukas, A.: The Last Deglaciation of the Southeastern Sector of the Scandinavian Ice Sheet, *Science*, 311, 1449–1453, 2006.
- Rommerskirchen, F., Eglinton, G., Dupont, L., and Rullkötter, J.: Glacial/interglacial changes in southern Africa: Compound-specific $\delta^{13}\text{C}$ land plant biomarker and pollen records from southeast Atlantic continental margin sediments, *Geochemistry, Geophysics, Geosystems*, 7, 2006.
- 645 Rostek, F. and Bard, E.: Hydrological changes in eastern Europe during the last 40,000yr inferred from biomarkers in Black Sea sediments, *Quaternary Research (United States)*, 80, 502–509, <http://dx.doi.org/10.1016/j.yqres.2013.07.003>, 2013.
- Schaefer, K., Lantuit, H., Romanovsky, V. E., Schuur, E. A., and Witt, R.: The impact of the permafrost carbon feedback on global climate, *Environmental Research Letters*, 9, 2014.
- 650 Schefuß, E., Eglinton, T. I., Spencer-Jones, C. L., Rullkötter, J., De Pol-Holz, R., Talbot, H. M., Grootes, P. M., and Schneider, R. R.: Hydrologic control of carbon cycling and aged carbon discharge in the Congo River basin, *Nature Geoscience*, 9, 687–690, 2016.
- Schneider Von Deimling, T., Grosse, G., Strauss, J., Schirrmeister, L., Morgenstern, A., Schaphoff, S., Meinshausen, M., and Boike, J.: Observation-based modelling of permafrost carbon fluxes with accounting for deep carbon deposits and thermokarst activity, *Biogeosciences*, 12, 3469–3488, 2015.
- 655 Schokker, J., Cleveringa, P., and Murray, A. S.: Palaeoenvironmental reconstruction and OSL dating of terrestrial Eemian deposits in the southeastern Netherlands, *Journal of Quaternary Science*, 19, 193–202, 2004.
- Schouten, S., Hopmans, E. C., and Sinninghe Damsté, J. S.: The organic geochemistry of glycerol dialkyl glycerol tetraether lipids: A review, *Organic Geochemistry*, 54, 19–61, <http://dx.doi.org/10.1016/j.orggeochem.2012.09.006>, 2013.
- 660 Schuur, E. A., Bockheim, J., Canadell, J. G., Euskirchen, E., Field, C. B., Goryachkin, S. V., Hagemann, S., Kuhry, P., Laffleur, P. M., Lee, H., Mazhitova, G., Nelson, F. E., Rinke, A., Romanovsky, V. E., Shiklomanov, N., Tarnocai, C., Venevsky, S., Vogel, J. G., and Zimov, S. A.: Vulnerability of permafrost carbon to climate change: Implications for the global carbon cycle, *BioScience*, 58, 701–714, 2008.
- Schuur, E. A., Vogel, J. G., Crummer, K. G., Lee, H., Sickman, J. O., and Osterkamp, T. E.: The effect of permafrost thaw on old carbon release and net carbon exchange from tundra, *Nature*, 459, 556–559, <https://doi.org/10.1038/nature08031>, 2009.
- 665 Schuur, E. A., McGuire, A. D., Schädel, C., Grosse, G., Harden, J. W., Hayes, D. J., Hugelius, G., Koven, C. D., Kuhry, P., Lawrence, D. M., Natali, S. M., Olefeldt, D., Romanovsky, V. E., Schaefer, K., Turetsky, M. R., Treat, C. C., and Vonk, J. E.: Climate change and the permafrost carbon feedback, *Nature*, 520, 171–179, 2015.

- Sidorchuk, A. Y., Panin, A. V., and Borisova, O. K.: Morphology of river channels and surface runoff in the Volga River basin (East European Plain) during the Late Glacial period, *Geomorphology*, 113, 137–157, 2009.
- 670 Sidorchuk, A. Y., Panin, A. V., and Borisova, O. K.: Surface runoff to the Black Sea from the East European plain during Last Glacial Maximum-Late Glacial time, *Special Paper of the Geological Society of America*, 473, 1–25, 2011.
- Simmons, C. T., Matthews, H. D., and Mysak, L. A.: Deglacial climate, carbon cycle and ocean chemistry changes in response to a terrestrial carbon release, *Climate Dynamics*, 46, 1287–1299, 2016.
- Sinninghe Damsté, J. S., Hopmans, E. C., Pancost, R. D., Schouten, S., and Geenevasen, J. A.: Newly discovered non-isoprenoid glycerol
675 dialkyl glycerol tetraether lipids in sediments, *Chemical Communications*, 17, 1683–1684, 2000.
- Soulet, G., Ménot, G., Bayon, G., Rostek, F., Ponzevera, E., Toucanne, S., Lericolais, G., and Bard, E.: Abrupt drainage cycles of the Fennoscandian Ice Sheet, *Proceedings of the National Academy of Sciences of the United States of America*, 110, 6682–6687, 2013.
- Stuiver, M. and Polach, H.: Reporting of ^{14}C data, *Radiocarbon*, 19, 355–363, 1977.
- Sun, S., Meyer, V. D., Dolman, A. M., Winterfeld, M., Hefter, J., Dumann, W., McIntyre, C., Montluçon, D. B., Haghypour, N., Wacker,
680 L., Gentz, T., Van Der Voort, T. S., Eglinton, T. I., and Mollenhauer, G.: ^{14}C Blank Assessment in Small-Scale Compound-Specific Radiocarbon Analysis of Lipid Biomarkers and Lignin Phenols, *Radiocarbon*, 62, 207–218, 2020.
- Svendsen, J. I., Alexanderson, H., Astakhov, V. I., Demidov, I., Dowdeswell, J. A., Funder, S., Gataullin, V., Henriksen, M., Hjort, C., Houmark-Nielsen, M., Hubberten, H. W., Ingólfsson, Ó., Jakobsson, M., Kjær, K. H., Larsen, E., Lokrantz, H., Lunkka, J. P., Lyså, A., Mangerud, J., Matiouchkov, A., Murray, A., Möller, P., Niessen, F., Nikolskaya, O., Polyak, L., Saarnisto, M., Siegert, C., Siegert, M. J.,
685 Spielhagen, R. F., and Stein, R.: Late Quaternary ice sheet history of northern Eurasia, *Quaternary Science Reviews*, 23, 1229–1271, 2004.
- Tesi, T., Muschitiello, F., Smittenberg, R. H., Jakobsson, M., Vonk, J. E., Hill, P., Andersson, A., Kirchner, N., Noormets, R., Dudarev, O., Semiletov, I., and Gustafsson: Massive remobilization of permafrost carbon during post-glacial warming, *Nature Communications*, 7, 1–10, 2016.
- Tisnérat-Laborde, N., Paterne, M., Métivier, B., Arnold, M., Yiou, P., Blamart, D., and Raynaud, S.: Variability of the northeast Atlantic
690 sea surface $\Delta^{14}\text{C}$ and marine reservoir age and the North Atlantic Oscillation (NAO), *Quaternary Science Reviews*, 29, 2633–2646, <http://dx.doi.org/10.1016/j.quascirev.2010.06.013>, 2010.
- Toucanne, S., Zaragosi, S., Bourillet, J. F., Cremer, M., Eynaud, F., Van Vliet-Lanoë, B., Penaud, A., Fontanier, C., Turon, J. L., Cortijo, E., and Gibbard, P. L.: Timing of massive 'Fleuve Manche' discharges over the last 350 kyr: insights into the European ice-sheet oscillations and the European drainage network from MIS 10 to 2, *Quaternary Science Reviews*, 28, 1238–1256, <http://dx.doi.org/10.1016/j.quascirev.2009.01.006>, 2009.
695
- Toucanne, S., Zaragosi, S., Bourillet, J. F., Marieu, V., Cremer, M., Kageyama, M., Van Vliet-Lanoë, B., Eynaud, F., Turon, J. L., and Gibbard, P. L.: The first estimation of Fleuve Manche palaeoriver discharge during the last deglaciation: Evidence for Fennoscandian ice sheet meltwater flow in the English Channel ca 20-18 ka ago, *Earth and Planetary Science Letters*, 290, 459–473, <http://dx.doi.org/10.1016/j.epsl.2009.12.050>, 2010.
- 700 Toucanne, S., Soulet, G., Freslon, N., Silva Jacinto, R., Dennielou, B., Zaragosi, S., Eynaud, F., Bourillet, J. F., and Bayon, G.: Millennial-scale fluctuations of the European Ice Sheet at the end of the last glacial, and their potential impact on global climate, *Quaternary Science Reviews*, 123, 113–133, 2015.
- Treat, C. C., Kleinen, T., Broothaerts, N., Dalton, A. S., Dommaine, R., Douglas, T. A., Drexler, J. Z., Finkelstein, S. A., Grosse, G., Hope, G., Hutchings, J., Jones, M. C., Kuhry, P., Lacourse, T., Lähteenoja, O., Loisel, J., Notebaert, B., Payne, R. J., Peteet, D. M., Sannel, A.
705 B. K., Stelling, J. M., Strauss, J., Swindles, G. T., Talbot, J., Tarnocai, C., Verstraeten, G., Williams, C. J., Xia, Z., Yu, Z., Väiliranta, M.,

- Hättestrand, M., Alexanderson, H., and Brovkin, V.: Widespread global peatland establishment and persistence over the last 130,000 y, *Proceedings of the National Academy of Sciences of the United States of America*, 116, 4822–4827, 2019.
- Turner, C.: The Eemian interglacial in the North European plain and adjacent areas, *Geologie en Mijnbouw/Netherlands Journal of Geosciences*, 79, 217–231, 2000.
- 710 Van Huissteden, J., Vandenberghe, J., Van Der Hammen, T., and Laan, W.: Fluvial and aeolian interaction under permafrost conditions: Weichselian Late Pleniglacial, Twente, eastern Netherlands, *Catena*, 40, 307–321, 2000.
- Vandenberghe, J. and Pissart, A.: Permafrost changes in Europe during the last glacial, *Permafrost and Periglacial Processes*, 4, 121–135, 1993.
- Vandenberghe, J., Renssen, H., Roche, D. M., Goosse, H., Velichko, A. A., Gorbunov, A., and Levvasseur, G.: Eurasian permafrost instability
715 constrained by reduced sea-ice cover, *Quaternary Science Reviews*, 34, 16–23, 2012.
- Vandenberghe, J., French, H. M., Gorbunov, A., Marchenko, S., Velichko, A. A., Jin, H., Cui, Z., Zhang, T., and Wan, X.: The Last Permafrost Maximum (LPM) map of the Northern Hemisphere: Permafrost extent and mean annual air temperatures, 25-17ka BP, *Boreas*, 43, 652–666, 2014.
- Vonk, J. E., Sanchez-Garca, L., Van Dongen, B. E., Alling, V., Kosmach, D., Charkin, A., Semiletov, I. P., Dudarev, O. V., Shakhova, N.,
720 Roos, P., Eglinton, T. I., Andersson, A., and Gustafsson, A.: Activation of old carbon by erosion of coastal and subsea permafrost in Arctic Siberia, *Nature*, 489, 137–140, 2012.
- Wacker, L., Christl, M., and Synal, H. A.: Bats: A new tool for AMS data reduction., *Nuclear Instruments and Methods in Physics Research Section B: Beam Interactions with Materials and Atoms*, 268, 976–979, 2010.
- Wainer, K., Genty, D., Blamart, D., Daëron, M., Bar-Matthews, M., Vonhof, H., Dublyansky, Y., Pons-Branchu, E., Thomas, L., van Calsteren,
725 P., Quinif, Y., and Caillon, N.: Speleothem record of the last 180 ka in Villars cave (SW France): Investigation of a large $\delta^{18}O$ shift between MIS6 and MIS5, *Quaternary Science Reviews*, 30, 130–146, 2011.
- Wang, M. J., Zheng, H. B., Xie, X., Fan, D. D., Yang, S. Y., Zhao, Q. H., and Wang, K.: A 600-year flood history in the Yangtze River drainage: Comparison between a subaqueous delta and historical records, *Chinese Science Bulletin*, 56, 188–195, 2011.
- Weltje, G. J. and Tjallingii, R.: Calibration of XRF core scanners for quantitative geochemical logging of sediment cores: Theory and
730 application, *Earth and Planetary Science Letters*, 274, 423–438, 2008.
- Winterfeld, M., Mollenhauer, G., Dummann, W., Köhler, P., Lembke-Jene, L., Meyer, V. D., Hefter, J., McIntyre, C., Wacker, L., Kokfelt, U., and Tiedemann, R.: Deglacial mobilization of pre-aged terrestrial carbon from degrading permafrost, *Nature Communications*, 9, 2018.
- Woronko, B., Rychel, J., Karasiewicz, T. M., Kupryjanowicz, M., Adamczyk, A., Fiłoc, M., Marks, L., Krzywicki, T., and Pochocka-Szwarc,
735 K.: Post-Saalian transformation of dry valleys in eastern Europe: An example from NE Poland, *Quaternary International*, 467, 161–177, 2018.
- Wu, J., Mollenhauer, G., Stein, R., Köhler, P., Hefter, J., Fahl, K., Grotheer, H., Wei, B., and Nam, S.-i.: Deglacial release of petrogenic and permafrost carbon from the Canadian Arctic impacting the carbon cycle, *Nature Communications*, 13, 1–11, 2022.
- Wu, L., Wilson, D. J., Wang, R., Yin, X., Chen, Z., Xiao, W., and Huang, M.: Evaluating Zr/Rb Ratio From XRF Scanning as an Indicator of Grain-Size Variations of Glaciomarine Sediments in the Southern Ocean, *Geochemistry, Geophysics, Geosystems*, 21, 2020.
- 740 Žák, K., Richter, D. K., Filippi, M., Živor, R., Deininger, M., Mangini, A., and Scholz, D.: Coarsely crystalline cryogenic cave carbonate—a new archive to estimate the Last Glacial minimum permafrost depth in Central Europe, *Climate of the Past*, 8, 1821–1837, 2012.

- Zhang, Y., Chiessi, C. M., Mulitza, S., Zabel, M., Trindade, R. I., Hollanda, M. H. B., Dantas, E. L., Govin, A., Tiedemann, R., and Wefer, G.: Origin of increased terrigenous supply to the NE South American continental margin during Heinrich Stadial 1 and the Younger Dryas, *Earth and Planetary Science Letters*, 432, 493–500, 2015.
- 745 Zhao, Z., Ahlberg, P., Thibault, N., Dahl, T. W., Schovsbo, N. H., and Nielsen, A. T.: High-resolution carbon isotope chemostratigraphy of the middle Cambrian to lowermost Ordovician in southern Scandinavia: Implications for global correlation, *Global and Planetary Change*, 209, 103751, 2022.
- Zhou, B., Zheng, H., Yang, W., Taylor, D., Lu, Y., Wei, G., Li, L., and Wang, H.: Climate and vegetation variations since the LGM recorded by biomarkers from a sediment core in the northern South China Sea, *Journal of Quaternary Science*, 27, 948–955, 2012.
- 750 Zimov, S. A., Davydov, S. P., Zimova, G. M., Davydova, A. I., Schuur, E. A., Dutta, K., and Chapin, I. S.: Permafrost carbon: Stock and decomposability of a globally significant carbon pool, *Geophysical Research Letters*, 33, 1–5, 2006.